Emilio Grande[1], Erin C. Seybold[2], Corianne Tatariw[3], Ate Visser[4], Anna Braswell[5, 6], Bhavna Arora[7], François Birgand[8], John Haskins[9], Margaret Zimmer[1]

[1] University of California Santa Cruz, Department of Earth and Planetary Sciences

[2] University of Kansas, Kansas Geological Survey

[3] University of Alabama, Department of Biological Sciences

[4] Lawrence Livermore National Laboratory, Nuclear and Chemical Sciences Division

[5] University of Florida, School of Forest Resources and Conservation, Fisheries and Aquatic Sciences Program

[6] University Florida Sea Grant, Institute of Food and Agricultural Sciences

[7] Lawrence Berkeley National Laboratory, Energy Geosciences Division

[8] North Carolina State University, Department of Biological and Agricultural Engineering

[9] Elkhorn Slough National Estuarine Research Reserve

Corresponding author: Emilio Grande (emgrande@ucsc.edu)

Key Points:

- Sub-hourly measurements of nitrate in salt marsh subsurface water show fluctuations in nitrate concentration at tidal frequencies.
- The nitrate-subsurface water level relationship forms hysteretic loops that explain nitrate transport and sources.
- Seasonal wet/dry changes cause significant shifts in salt marsh biochemical behavior, and nitrate retention mainly occurs in dry periods.

Abstract

Salt marshes remove terrestrially derived nutrients en route to coasts. While these systems play a critical role in improving water quality, we still have a limited understanding of the spatiotemporal variability of biogeochemically reactive solutes and processes within salt marshes. To investigate this knowledge gap, we implemented a high-frequency sampling system to monitor sub-hourly nitrate (NO_3^-) concentrations in salt marsh porewater at Elkhorn Slough in central California, USA. We instrumented three marsh positions along an elevation gradient subjected to different extents of tidal inundation, which we hypothesized would lead to varied biogeochemical characteristics and hydrological interactions. At each marsh position, we continuously monitored NO_3^- concentrations at depths of 10, 30, and 50 cm with subsurface water levels measured from 70 cm wells over seven deployments of ~10 days each. We quantified tidal event hysteresis between NO_3^- and water level to understand how

NO_3^- concentrations and sources fluctuate across tidal cycles. There was significant differences in the NO_3^--subsurface water level hysteresis patterns across seasonal wet/dry periods common to Mediterranean climates. In dry periods, the NO_3^--subsurface water level relationship indicated that the NO_3^- source was likely estuarine surface water that flooded the transect during high tides. In wet periods, the NO_3^--subsurface water level relationship suggested the salt marsh was a source of NO_3^-. These findings suggest that tidal and seasonal hydrologic fluxes control NO_3^- porewater dynamics and influence ecological processes in coastal environments.

Plain Language Summary

Salt marshes are at the land-sea interface. They can filter pollutants, particularly nitrogen species, as water moves into the ocean. However, we do not know how the processes that remove and transport nitrate change with space and time, especially over hourly timescales. To improve our understanding of nitrate variations in these types of environments, we conducted a study in a salt marsh in California where we measured nitrate at high-frequency intervals at different marsh sediment depths.

We observed that subsurface nitrate concentrations fluctuate during tidal cycles, even at deeper depths, and marked seasonal wet/dry changes common to California's climate caused significant seasonal shifts in the nitrate-subsurface water level relationship. In dry periods, the nitrate-subsurface water level relationship indicated that the nitrate source was likely estuarine surface water that flooded the transect during high tides. In wet periods, the nitrate-subsurface water level relationship suggested the salt marsh was a source of nitrate. Our work highlights the dynamic variability in nutrient processing and the critical role of seasonality in driving observed water quality patterns.

1 Introduction

Salt marsh systems act as buffers at the terrestrial-marine interface, whereby terrestrially derived nutrients may be retained or processed in salt marshes, potentially reducing the impacts of these pollutants on coastal environments (Kumar et al., 2019; Reading et al., 2017). These processes are critical as excess nutrients, especially nitrate (NO_3^-), discharged to coastal estuaries can drive eutrophication and hypoxia (Peterson et al., 2016), which may worsen with expected shifts in climatic patterns (Sinha et al., 2017). Despite the importance of the biogeochemical reactivity of salt marshes, we have a limited understanding of the spatiotemporal variability of critical biogeochemically reactive solutes and processes. Specifically, there is a knowledge gap in the short-term dynamics of NO_3^- in subsurface water at timescales over which NO_3^- can be transported, retained, and removed.

Hydrology, including the bidirectional water inputs from both land and sea into the marsh, such as tidal water, subsurface water, and terrestrial groundwater,

is a potential driver of nutrient delivery and cycling in salt marsh porewater (Krause et al., 2020). For example, water fluxes across the sediment-water interface control the exchange of nutrients, such as NO_3^-, from tidally driven surface water exchanges into salt marsh porewater (Santos et al., 2012; Wang et al., 2022). However, the NO_3^-concentrations in salt marsh porewater at intra-tidal timescales and their relationship with subsurface water levels are not entirely understood (Caetano et al., 2012). Available datasets of NO_3^- and other biogeochemical parameters in salt marshes are usually limited to short-term synoptic sampling campaigns or infrequent long-term sampling, often with limited spatial resolution. Therefore, we have historically understudied short-term and fine-scale porewater NO_3^- dynamics over more than a few tidal cycles in these ecosystems. For example, impacts of short-lived, episodic events such as storms and tidal inundation can drive biogeochemical parameters (Grande et al., 2022), but may be missed by coarse resolution sampling.

Quantifying the dynamic relationship between tidal inundation and NO_3^-in salt marshes can improve our understanding of dominant NO_3^- transport pathways, as well as biogeochemical sources and retention processes. This relationship has been studied through synoptic sampling of tidal events and analyzing the variations of NO_3^- and water level with time (Caetano et al., 2012; Wang et al., 2022). Previous work has found that the biogeochemical behavior of salt marshes can change as a function of tidal inundation, with shifts between retaining and producing NO_3^-during low neap and spring tides, respectively (Caetano et al., 2012). However, these inferences have been based on a limited number of tidal events and in a single season. Thus, we lack understanding of whether and how salt marshes transition between being a NO_3^- source and a NO_3^- sink. In riverine environments, solute concentration-discharge (i.e., c-Q) relationships have been observed to have hysteretic behavior and have been used to infer changing solute sources and transport processes (Arora et al., 2020; Chanat et al., 2002). Hysteresis occurs when the c-Q relationship is different on the rising limb of a storm hydrograph versus the falling limb (Aguilera & Melack, 2018; Chanat et al., 2002). A clockwise relationship (NO_3^- concentrations are lower on the falling limb versus the rising limb) is thought to be the result of a limited NO_3^- supply close to the measurement location (Zuecco et al., 2016). A counterclockwise hysteresis pattern occurs when the NO_3^- concentrations are higher on the falling limb versus the rising limb. This nonlinear relationship may be observed when the NO_3^- sources have a longer transport time (Bieroza & Heathwaite, 2015). For this study, we propose to apply this analysis approach commonly used in riverine systems to better understand NO_3^-dynamics in a salt marsh. When applied to a salt marsh, hysteresis may occur when the NO_3^--water level relationship differs on the rising limb of the high tide versus the falling limb as the tide retreats.

We propose that hysteresis relationships can indicate the general sources and sinks of NO_3^- during tidal events, for example, if NO_3^- is tidally sourced or if it is produced or consumed in the salt marsh. Several processes can increase or decrease NO_3^- concentrations in salt marshes over tidal cycles. Notably, salt

marshes can produce NO_3^- via nitrification, the biological oxidation of ammonia (NH_3) or ammonium (NH_4^+) to NO_3^- (Devol, 2015). In coastal estuaries, surface NH_4^+ concentration can be elevated, favoring nitrification (Hicks et al., 2019). Further, processes such as denitrification, the reduction of NO_3^- to gaseous forms of nitrogen under anoxic conditions (Almaraz et al., 2020), which is common in salt marsh systems (Addy et al., 2005), can result in a decrease in NO_3^-concentrations in salt marsh porewater over tidal cycles. Quantification of NO_3^--water level relationships could serve as a valuable tool to improve understanding of transport and processing dynamics in coastal areas. We hypothesize that in shallow subsurface water within the salt marsh, a clockwise loop indicates that the incoming tide is likely a source of NO_3^-. That is, as the tide floods the transect, we would observe higher pore water NO_3^- concentrations in the rising versus the falling limb. Conversely, a counterclockwise loop with higher concentrations on the falling limb may indicate that the salt marsh could be a source of NO_3^- during ebbing tides or low tidal periods.

In situ water quality sensors have given us access to high-frequency measurements in many environmental systems. However, their cost prohibits the installation of many needed to obtain high spatial resolution observations. Birgand et al. (2016) have provided a solution by creating a multiplexed pumping system (MUX, MultiplexÔ llc) which sequentially pumps water from up to 12 sources to one high-frequency sensor. Coupled with a field-deployable spectrophotometer, they have shown that it is possible to obtain high-frequency measurements of NO_3^- across space or on a replicated manner for lab experiments (Birgand et al., 2016). In particular, they used this tool to show that velocity of water flowing over wetland sediment has a major impact on sediment denitrification, likely because of enhanced exchange between the two (Birgand et al., 2016). This setup was applied for subsurface sampling in an agricultural drained soil, coupling a spectro::lyser (S::CAN) to the MUX (MultiplexÔ, llc) from a network of shallow groundwater wells to evaluate the spatiotemporal variability of nitrate at sub-hourly timescales for three depths and three distances to the drain (Liu et al., 2020). These techniques offer exciting opportunities for understanding NO_3^-dynamics in salt marshes, where intertidal variations could cause relatively rapid changes in marsh porewater biogeochemistry (Grande et al., 2022).

To advance our understanding of nutrient dynamics in salt marshes, we implemented the novel MUX system coupled with a field-based spectrophotometer to monitor sub-hourly porewater NO_3^- concentrations at multiple elevations and depths within a marsh (Birgand et al., 2016). Specifically, we used the high spatiotemporal resolution NO_3^- data to study multi-scale hydrologic controls on marsh porewater NO_3^- concentration by investigating: (1) how tidal dynamics impact short-term variations in porewater NO_3^-; (2) how seasonality (i.e., wet versus dry seasons) modulates the impact of tidal cycles on NO_3^- dynamics; and (3) how potential NO_3^- sources and transport processes drive NO_3^- concentrations in salt marsh subsurface water.

2 Study area and measurements

2.1 Study site description

This study was conducted at Elkhorn Slough in Monterey Bay, California (Figure 1A), which is part of the National Estuarine Research Reserve System (NERR). The principal sources of freshwater to Elkhorn Slough are the Old Salinas River, a perennial stream that discharges at the mouth of the slough, and Carneros Creek, an intermittent stream that only flows during the wet winter months (J. M. Caffrey & Broenkow, 2002). Tides in the estuary are mixed semidiurnal with a mean range of 1.7 m, a spring tidal range of 2.5 m, and a neap tidal range of 0.9 m. The principal transport mechanism for water in Elkhorn Slough occurs via tidal exchange (J. M. Caffrey & Broenkow, 2002). Monterey Bay seawater reaches up to 6 km inland during high tides, and over 50% of the total water volume of the slough is flushed during each tidal cycle (Malzone, 1999).

Agricultural development in the watershed around Elkhorn Slough has increased in recent decades, leading to elevated nutrient concentrations, especially nitrogen species, in surface waters (Van Dop et al., 2019). The Old Salinas River and Moro-Cojo Slough drain intensely farmed areas and discharge at the southern end of Moss Landing Harbor (Jane M. Caffrey et al., 2002). These NO_3^--rich waters result in significant sources of NO_3^- at the mouth of Elkhorn Slough that is transported into the slough with the tides (Hicks et al., 2019). The high NO_3^- concentration observed at Moss Landing Harbor (Figure 1A) result in rapid consumption via denitrification (Almaraz et al., 2020), and photosynthetic uptake as the water mixes inside the estuary (Chapin et al., 2004). Further, dissimilatory NO_3^- reduction to ammonium (DNRA), the anaerobic respiration by chemoorganoheterotroph microbes using NO_3^- as an electron acceptor for respiration and reducing NO_3^- to NH_4^+, results in elevated surface water NH_4^+ concentration in the upper sections of the Slough (Jane M. Caffrey et al., 2002; Jeppesen et al., 2018), where the field site for the present study is located (black star in Figure 1A). Studies have also linked problematic surface water nutrient concentrations in Elkhorn Slough to climatic drivers, such as precipitation (Hicks et al., 2019), with more significant NO_3^- and NH_4^+ concentration observed during rainy winter and spring months due to runoff from agricultural fields (Supporting information Figure S1). Further, Elkhorn Slough has been designated as a moderately eutrophic estuary and high eutrophic expression close to the study site (Hughes et al., 2011).

The average precipitation at Elkhorn Slough is 627 mm/year (based on 2001-2020 record collected by the NERR ~4.5 km from the study site), with ~ 90% of the precipitation falling between November and April as rain (Chapin et al., 2004). Air temperature averages 11.1 °C in the winter and 15.4 °C in the summer (J. M. Caffrey, 2002). The Mediterranean climate results in marked wet/dry seasonal dynamics (Figure 2), which provide the conditions to resolve seasonal variations in climatic forcing that impact subsurface saturation and biogeochemical conditions. In this area, the wet periods occur during the dormant winter season, while the dry periods occur during the summer growing

season. Pickleweed, *Salicornia pacifica*, is the dominant marsh plant (Van Dyke & Wasson, 2005), and the dominant grazer and bioturbator is the lined shore crab, *Pachygrapsus crassipes* (Beheshti et al., 2022).

To explain the temporal variations in NO_3^- concentrations in subsurface marsh sediments, we used surface water pH, salinity, dissolved oxygen, temperature, and turbidity, available through the NERR. The NERR, in partnership with the National Oceanographic and Atmospheric Administration maintains a tidal gauge at the mouth of the slough (Figure 1A). In addition to surface water level (tidal elevation), surface water salinity, pH, dissolved oxygen, and turbidity are available.

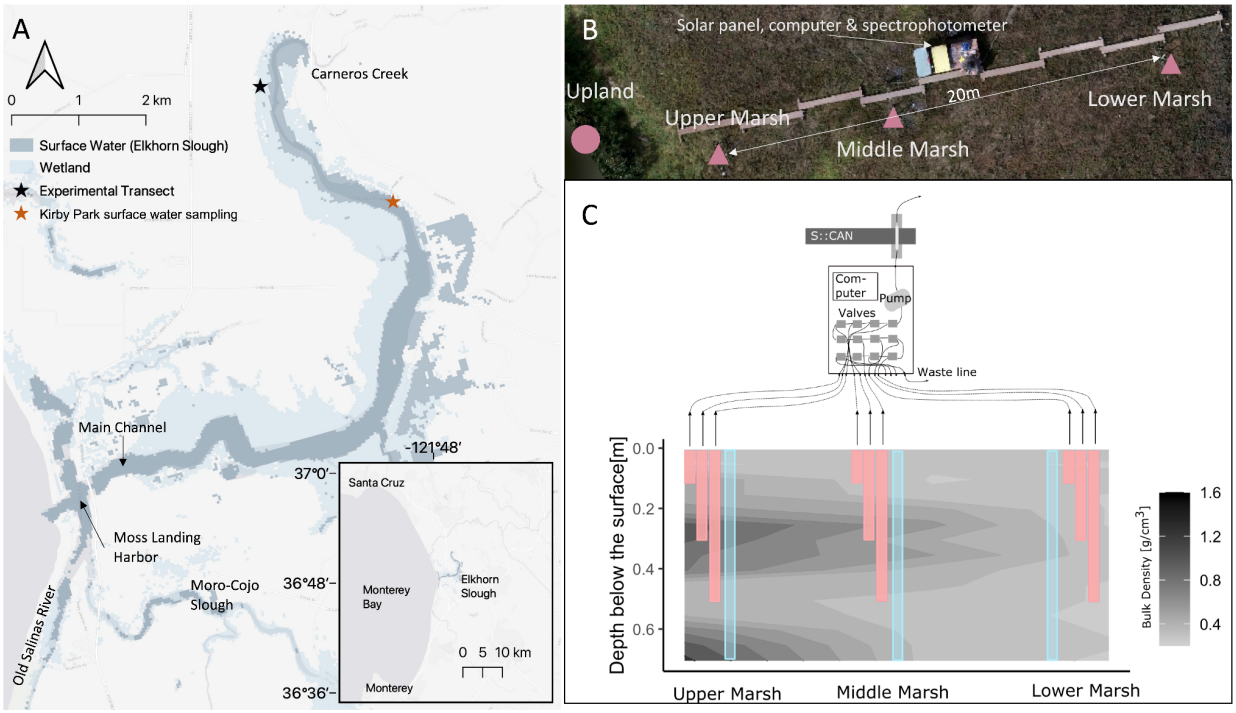

Figure 1. (a) Map of Elkhorn Slough with the extent of wetlands outlined in light blue. The black star marks the location of the study transect. The orange star marks the location of the Kirby Park, where the ESNERR collects monthly estuarine surface water samples that are analyzed for NO_3^- and NH_4^+ concentration. (b) Map view of the experimental transect showing the location of the upland monitoring piezometer in relation to the salt marsh transect. (c) Cross section illustration of the experimental transect showing the spatial distribution of the sampling cups (pink bars) and observation wells (blue bars) with a contour plot overlay of sediment bulk density across the salt marsh. The darker the colors in the contour plot, the greater the bulk density. The elevation (m amsl; not shown in the figure) of the salt marsh positions are: 1.79 m, 1.65 m, and 1.55 m for the upper, middle, and lower marsh, respectively.

2.2- Experimental transect

For this study, we instrumented a 25 m experimental transect in an emergent tidal wetland with an elevation range of 0.24 m (Figure 1). We delineated the transect into upper, middle, and lower marsh positions through elevation surveys and inundation extents (supporting information Figure S2; Figure 1B). The elevations above mean sea level of the upper, middle, and lower marsh are 1.79 m, 1.65 m, and 1.55 m, respectively. These elevations are tidally inundated 6.7%, 8.9%, and 11.2% of the time, respectively, based on subsurface water level data collected at the site between February 2019 and November 2021. This wetland elevation categorization coincides with previous delineations of salt marsh zones across the Elkhorn Slough estuary based on vegetation coverage and elevation (Woolfolk & Labadie, 2012), and are thus broadly representative.

Sediment bulk density varies with elevation and depth at the site. Bulk density increases from the surface to 30 cm depth, then from 30 to 50 cm bulk density resembles that of the surface (Figure 2.1C). Sediment bulk density decreased from the upper marsh to the lower marsh positions, with mean values of 0.92 g/cm^3 and 0.22 g/cm^3, respectively.

We installed and maintained a network of observation wells at each marsh position to measure subsurface water level variations (Figure 1C). We installed the wells to a depth of 70 cm below the surface by pushing drive-point PVC pipes directly into the ground to minimize gaps around the pipe, which could cause water movement vertically along the well's annulus. We screened the wells from 5 cm below the ground surface to the total depth. We recorded water level and temperature in these wells with Solinst pressure transducer loggers (Ontario, Canada) at 5-minute intervals. We also measured air pressure at the transect at 5-minute intervals to barometrically correct the pressure transducer measurements to allow calculation of water level. We coupled these wells with high frequency measurements of porewater NO_3^- concentration using an *in-situ* sensor system described in the next section.

We installed a deep piezometer to 3.5 m below the ground surface, with 15-cm screen at the base, in an upland location ~5 m uphill from the upper marsh, which is not tidally inundated (Figure 2.1B). We used the same Solinst set up to measure groundwater levels at 5-minute intervals to quantify water level variations and evaluate the potential for fresh subsurface water to move laterally towards the salt marsh.

2.3- Water quality measurements

To measure high frequency variations in porewater NO_3^- concentration, we coupled a multisource pump system with a field-based spectrophotometer (S::CAN Spectro::lyser ™; (Birgand et al., 2016; Liu et al., 2020). We connected the MUX to nine sampling cups installed to depths of 10, 30, and 50 cm at each marsh position (Figure 1C). We designed the sampling cups to be similar to those described in Liu *et al.*, (2020a). The sampling cups are a "closed" chamber with

an approximate volume of 150 mL (volume varied considering the depth of the sampling cup), which held enough water to rinse the optical path and allow sufficient water for an accurate measurement (Birgand et al., 2016). For each cup, we used a 6-8 cm length of 5 cm internal diameter (I.D.) screened PVC pipe capped at the bottom end with a PVC cap and an epoxy resin plug at its top end (supporting information Figure S3). We installed tubing (0.5 cm I.D.) from the bottom of the sampling cup through the sealed epoxy layer to connect the sampling cup to the MUX. We installed 51 micron in-line filters at the connection of the tubing with the MUX to reduce large particles from clogging the system, and minimize fouling potential in the MUX and the optical probe. For the sampling cups, we used an additional vent of equal internal diameter to prevent a vacuum forming during pumping, provide hydrostatic equilibrium with the surrounding water table in the cup, and provide an escape for air as water entered the cup (supporting information Figure S3). When installed, we placed washed sand around the sampling cups to avoid flow restriction towards the cups. Given the low permeability of the native sediment, we placed compacted native sediment above the sand layer to avoid sampling water from above the sampling cup depth.

The MUX pumped porewater from the sampling cups to a 4 mL quartz flow-through cuvette with a 10 mm pathlength (Starna-cell , model 46-Q-10) attached to the optical probe (Figure 1C). We set the temporal resolution of NO_3^- concentration measurements to ~50 minutes for each measuring cycle. In each measuring cycle, we measured the empty cuvette (e.g., took an air absorbance measurement of the empty cuvette) to monitor any potential optic fouling of the cuvette over time (Etheridge et al., 2014). We also flushed the cuvette with deionized water to remove chemical fouling once per measuring cycle. Lastly, we pumped and purged a cleaning solution (12 mg/L oxalic acid) to minimize the cuvette's chemical fouling during each sampling event. The MUX has logging capabilities and we stored the time stamp, the corresponding valve number, and 216 absorbance measurement values for each optical probe measurement (200 nm to 737.5 nm, 2.5 nm resolution).

We deployed the optical sensor coupled with the MUX in seven deployment periods of ~ten days each, between January and October 2021 (Figure 2). Data gaps during deployments represent sampling cup or instrument malfunctions, resulting in different amounts of data for some marsh positions or depths (supporting information Table S1).

For this study, we also used available surface water quality data through the Elkhorn Slough National Estuarine Research Reserve (ESNERR). The most reliable, closest sampling station to the research site is Kirby Park, 2.1 km for our site (Figure 1A), where monthly surface water NO_3^- and NH_4^+ concentration data are available for the study period (January-October 2021).

3 Methodology

3.1- In situ nitrate measurements and data preparation

We created and employed a site-specific calibration model to estimate NO_3^- concentrations using the spectral data from the optical probe. Across all deployment periods, we collected a total of 91 grab samples as water flowed through the cuvette paired with the optical probe measurement. We analyzed these samples for NO_3^- concentration using a Lachat Quickchem 8500 auto-analyzer at the Marine Analytical Lab at the University of California, Santa Cruz, following the EPA 353.2 method (O'Dell, 1996). These samples comprised our calibration library, which we used in combination with the absorbance spectra from the optical probe to estimate NO_3^- using Partial Least Square Regression (PLSR; (Etheridge et al., 2014), through the pls package in R (Liland et al., 2021). This calibration model was then applied to the entire time series of absorbance spectra. More than 99% of the variance in laboratory measured NO_3^- concentration was explained by the sensor data. The Nash–Sutcliffe efficiency of the model was 0.88 and the root mean square error of the prediction was 0.09 mg/L (Supporting Information Figure S4). We generated NO_3^- concentration times series for each instrument deployment period using the calibration model. We filled short data gaps (<4 h) using cubic spline interpolation and produced a continuous time series to analyze tidal events.

To better capture the dimension and direction of NO_3^--subsurface water level relationship (i.e., get the water level and NO_3^- concentration datasets on the same time step), we used a locally estimated scatterplot smoothing (LOESS) with a minimal smoothing parameter (α) of 0.1 to smooth the NO_3^- concentration time series closely to the data (e.g., supporting information Figure S5).

3.2- Tidal events delineations

For each deployment period, we delineated individual tidal events, which we defined as the periods when the water level in the observation wells increased and then decreased as a function of individual tidal cycles (Figure 3). We only delineated tidal events that inundated the top of the salt marsh. Thus, we did not identify any tidal event during the May deployment because the site was never inundated (Supporting Information Table S1). Differences in elevation across the salt marsh, where higher elevation sites were inundated less frequently, resulted in different numbers of tidal events at each marsh position. Furthermore, instrument failure during some deployments resulted in differences in the number of tidal events studied for individual depths and marsh positions. We delineated 158 tidal events, including 58 at the lower marsh, 43 at the middle marsh, and 57 at the upper marsh position (Figure 7).

Of the 158 tidal events, 65% of them occurred during the wet season (January to May 2021) and 35% occurred during the dry season (July to October 2021; Table S1).

3.3- Analyses of hysteresis indices

We used hysteresis indices to quantify temporal porewater NO_3^- concentration-subsurface water level relationships for each tidal event across marsh positions (Lloyd et al., 2016). We used the subsurface water level measured in the observation wells at individual marsh positions (Figure 1C). The hysteresis index has been widely used, and there is a robust description of this analysis in the literature (Andrea et al., 2006; Liu et al., 2021; Vaughan et al., 2017). In brief, the hysteresis index (*HI*) is based on normalized water level and NO_3^- concentration as:

$$h_{i-\ norm} = \frac{h_i - h_{\min}}{h_{\max} - h_{\min}} \quad (1)$$

$$C_{i-\ norm} = \frac{C_i - C_{\min}}{C_{\max} - Q_{\min}} \quad (2)$$

Where h_i and C_i are the water level and NO_3^- concentration values at time step *i*, h_{max} and h_{min} are the maximum and minimum water levels in the tidal event, and C_{max} and C_{min} are the maximum and minimum NO_3^- concentration in the tidal event. We normalized NO_3^- and water levels between 0 and 1 to facilitate the comparison of indices across tidal events because this ensures all events are evaluated on the same scale (Lloyd et al., 2016).

Further, we calculated the hysteresis index for each water level interval (HI_j) as:

$$\mathrm{HI}_j = C_{j-rising} - C_{j-falling} \quad (3)$$

Where $C_{j-rising}$ and $C_{j-falling}$ are calculated by estimating C_{i-norm} at 1% intervals of h_{i-norm} on the rising and falling limbs through linear regression of two adjacent values C_{i-norm} (Kincaid et al., 2020; Vaughan et al., 2017). We calculated the mean HI_j value for each tidal event to determine an event-specific hysteresis index (Figure 4). The *HI* values range between −1 and 1. Negative values indicate counterclockwise hysteresis and positive values indicate clockwise hysteresis. The magnitude of *HI* is the normalized difference between the rising and falling limbs of a flooding high tide (Figure 4). *HI* close to zero represents less hysteresis (i.e., *HI*'s magnitude influences the size of the loop).

We also calculated Flushing Index values for each tidal event (*FI*, Figure 4C). The *FI* is computed as the slope of the line between the normalized subsurface water level value at the peak tidal event (i.e., the maximum normalized subsurface water level value) and the normalized subsurface water level value at the beginning of the tidal event (Vaughan et al., 2017). Values of this index range between −1 and 1 (Figure 4C). Negative values indicate a decrease in NO_3^- concentrations on the rising limb whereas positive values indicate an increase in NO_3^- on the rising limb. The distance from zero indicates the magnitude of the difference in NO_3^- concentration at the start of the tidal event and the peak of the tidal event. A positive *FI* could suggest that the salt marsh is a source of NO_3^- or that tidal water "flushes" the salt marsh subsurface with high NO_3^-, and we observe it as an increase in NO_3^- on the rising limb of the event. A negative *FI* would imply that the tidal water is a source of NO_3^-, which is consumed

in the salt marsh over the tidal event, resulting in a decrease in NO_3^- from the beginning of the high tide towards the maximum water level. A negative FI can also result from dilution processes if the incoming tidal water dilutes the salt marsh subsurface from the beginning to the peak of the tidal event.

4 Results

4.1- Precipitation, seasonal groundwater level and salt marsh subsurface water level fluctuations

Water year 2020 was extremely dry, with 281 mm of total precipitation, which was 346 mm below the long-term annual average for the area. Over the study period, we observed a difference of 1.34 m between the peak terrestrial groundwater level (2.75 m-amsl) in the wettest period (December 2020) and the lowest level (1.39 m-amsl) in the driest period (September 2021).

The terrestrial water level responds to precipitation events with relative increases during precipitation periods (Figure 2). Marsh subsurface water levels are subject to daily, biweekly, and seasonal tidal cycle inundation dynamics (due to the position of the moon/earth), resulting in multiple water level fluctuation frequencies (Grande et al., 2022). Subsurface water levels at the lower marsh position are consistently lower than at the upper and middle marsh positions during low tides, draining below the marsh surface elevation in each tidal cycle. However, the subsurface water level in the upper and middle marshes did not drop below the marsh elevation during the wet dormant season (e.g., January to March 2021; Figure 2). This indicates that this portion of the marsh does not drain substantially between daily tidal cycles during this period. As the system transitioned into the dry season, we observed that the terrestrial groundwater levels decreased, and the salt marsh subsurface water levels dropped below the salt marsh surface between tidal inundation periods (e.g., April to October 2021; Figure 2).

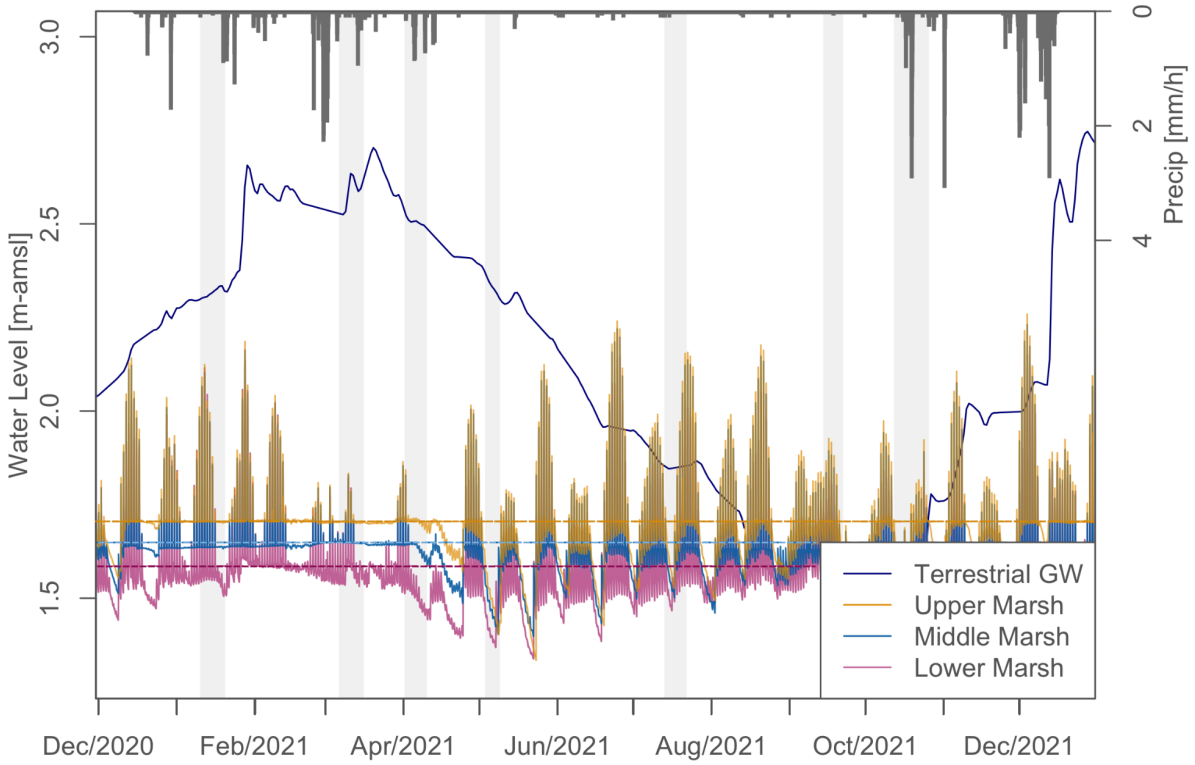

Figure 2. Water level time series illustrating the seasonal variations of the terrestrial groundwater level (dark blue) as measured from the upland study location. The Mediterranean climate of the study area, with marked seasonality in precipitation (gray hanging bars), results in a drop of 1.34 m in the terrestrial groundwater level between the rainy and dry seasons. The figure also illustrates the subsurface water level time series in the upper (yellow), middle (light blue), and lower (pink) marsh positions. The horizontal dashed lines represent the salt marsh elevation at each marsh position (by color). The shaded regions mark the instrumentation deployment periods.

4.2- Effect of salt marsh position and depth on porewater nitrate concentrations

NO_3^- concentration in salt marsh porewater ranged between 0 and ~1 mg/L over the study period, with a mean and a standard deviation of 0.17 mg/L and 0.12 mg/L, respectively. Overall, we found differences in NO_3^- concentrations across the different marsh positions and different depths, but these differences were complex and did not follow simple trends with marsh elevation. Temporal variations in NO_3^- concentration differed between marsh positions (Brown-Forsythe test: $F(2) = 680.41$, $p < 0.0001$; Table 1; Figure 5A), with the upper marsh

position showing the greatest temporal variability (Interquartile range, IQR = 0.22 mg/L). Overall, the middle marsh had higher porewater NO_3^- concentrations (median = 0.19 mg/L) than the lower (median = 0.14 mg/L) and upper marsh positions (median = 0.14 mg/L; Kruskal-Wallis test: H = 479.14, df = 2, $p < 0.0001$; Table 1, Figure 5A).

Temporal variations in NO_3^- concentration also differed between depths (Brown-Forsythe test: F(2) = 211.95, $p < 0.0001$; Figure 5B), with the 50 cm depth showing the greatest temporal variability (IQR = 0.17 mg/L). The NO_3^- concentration at 50 cm depth were significantly higher (median = 0.19 mg/L) than at 10 cm (median = 0.15 cm) and 30 cm depths (median = 0.13 mg/L; Kruskal-Wallis test: H = 659.33, df = 2, $p < 0.0001$; Table 1, Figure 5B).

Marsh Position	**Mean NO_3 [mg/L]**	**Median NO_3 [mg/L]**	**SD NO_3 [mg/L]**	**IQR NO_3 [mg/L**
Lower	0.15	0.14	0.10	0.14
Middle	0.19	0.19	0.12	0.151
Upper	0.18	0.14	0.15	0.22
Depth [cm]				
10	0.167	0.15	0.12	0.15
30	0.15	0.13	0.11	0.15
50	0.20	0.19	0.13	0.18

Table 1. Summary statistics for the different marsh positions and across all depths of the experimental transect. SD is the standard deviation and IQR is the interquartile range (i.e., the range between the 25^{th} and 75^{th} quartiles).

The effect of depth on NO_3^- concentration varied between individual marsh positions, with the highest concentrations occurring at different depths in each position. At the lower marsh position, median NO_3^- concentration was highest at 30 cm depth (median = 0.157 mg/L; Kruskal-Wallis test: H= 21.21, df = 2, $p < 0.0001$), and there was no difference between the 10 cm (median = 0.134 mg/L) and 50 cm depths (median = 0.133 mg/L; Kruskal-Wallis test: H= 0.67, df = 1, p = 0.4) (Figure 5D). In contrast, in the middle marsh, the median NO_3^- concentration was lowest at the 50 cm depth (median = 0.15 mg/L; Kruskal-Wallis test: H= 197.17, df = 2, $p < 0.0001$). There was no difference between the 10 cm (median = 0.21 mg/L) and 30 cm depths (median = 0.23 mg/L; Kruskal-Wallis test: H= 3.17, df = 1, p = 0.075; Figure 5E). Finally, at the upper marsh, median NO_3^-concentrations varied between all depths, with the highest concentrations occurring at the 50 cm depth (median = 0.27 mg/L) and the lowest at the 30 cm depths (median = 0.06 mg/L; Kruskal-Wallis test: H= 1823.4, df = 2, $p < 0.0001$; Figure 5F).

4.2.1 Seasonal effects on nitrate concentration

Although the effect of marsh position and depth on NO_3^- concentrations was complex, we found clearer and more consistent differences in porewa-

ter NO_3^- concentrations between wet and dry periods. There were higher NO_3^- concentrations during wet periods (median = 0.21 mg/L) than during dry periods (median = 0.10 mg/L; Kruskal-Wallis test: H = 1328.5, df = 1, p < 0.0001) across all marsh positions and depths (Figure 5G-H). We also found an effect of wet/dry seasons on porewater NO_3^- concentrations among depths across the salt marsh, with higher NO_3^- concentration in the wet season (Table 2).

However, the effect of wet/dry season on depth varied between individual marsh positions. At the lower and middle marsh positions, NO_3^- concentrations were higher at all depths during the wet season (Table 3). In contrast, at the upper marsh position, NO_3^- concentrations were lower at the 10 cm and 30 cm depths during the wet season relative to the dry season. At the 50 cm depth, NO_3^- concentrations were higher during the wet season relative to the dry season (Table 3).

Marsh Position	**Median dry season NO_3 [mg/L]**	**Median wet season NO_3 [mg/L]**	**Kruskal-W**
Lower	0.08	0.19	507.6
Middle	0.11	0.24	499.4
Upper	0.10	0.17	104.4
Depth [cm]			
10	0.11	0.20	144.5
30	0.10	0.18	183.7
50	0.09	0.24	1198.6

Table 2. Summary statistics of seasonal salt marsh porewater NO_3^- concentrations. Wet season NO_3^- concentrations are significantly higher in all the marsh positions and depths of this study. All tests in the table have 1 degree of freedom and p-value < 0.0001.

4.3- Estuarine surface water nitrate and ammonium concentrations

During the study period, monthly measurements of estuarine surface water NO_3^- concentration varied between 0.08 mg/L in summer (June 2021) and 2.9 mg/L in the winter (February 2021). Over the study, surface water NO_3^- had a mean, median, standard deviation, and interquartile range (IQR) of 0.46 mg/L, 0.13mg/L, 0.86mg/L, and 0.23 mg/L, respectively (Figure 5C).

Surface water NH_4^+ concentration varied between 0.06 mg/L in summer (June 2021) and 0.36 mg/L in the winter (February 2021). Surface water NH_4^+ had a mean, median, standard deviation, and IQR of 0.09 mg/L, 0.07 mg/L, 0.11 mg/L, and 0.07 mg/L, respectively (Figure 5C).

Marsh Position	**Depth [cm]**	**Median dry season NO_3 [mg/L]**	**Median wet season NO_3 [mg/L**

Lower	10	0.13	0.19
Lower	30	0.09	0.19
Lower	50	0.04	0.20
Middle	10	0.12	0.24
Middle	30	0.12	0.22
Middle	50	0.07	0.25
Upper	10	0.11	0.06
Upper	30	0.10	0.05
Upper	50	0.10	0.34

Table 3. Summary statistics of seasonal effects on NO_3^- concentrations by depth in each marsh position. All tests in the table have 1 degree of freedom and p-value < 0.0001

4.4 Hysteresis Index

Tidal event *HI* values were influenced by season (Figure 7C; Kruskal-Wallis test: H= 31.43, df = 1, $p < 0.0001$) rather than marsh position (Kruskal-Wallis test: H= 2.328, df = 2, p = 0.3) or depth (Kruskal-Wallis test: H= 3.74, df = 2, p = 0.15). Median *HI* was predominantly negative (counterclockwise) during the wet season (median = -0.13), contrasting with a predominantly positive (clockwise) *HI* during the dry season (median = 0.15). However, this seasonal effect did not persist across all marsh positions and depths.

The effect of seasonality on hysteresis patterns was evident across depths in the upper marsh position, with significant differences between wet and dry periods at all depths (Table 4). Predominantly positive *HI* in the dry season contrasted with predominantly negative *HI* in the wet season. There was no effect of season at any depth in the middle marsh position (Table 4). In the lower marsh, *HI* was negative during the wet season and positive during the dry season for the 10 cm and 50 cm depths, with significant differences among wet and dry periods (Table 4). Conversely, the *HI* in the 30 cm depth of the lower marsh was not significantly different among the dry and wet seasons (Table 4).

Dispersion in *HI* differed significantly between wet and dry periods for the middle marsh (Brown-Forsythe test: $F(1) = 6.5$, $p = 0.015$) with the wet season displaying a larger scattering than the dry season (Figure 7). We did not find significant differences in the scattering between wet and dry seasons for the upper (Brown-Forsythe test: F(1) = 0.1, p =0.7) or lower marsh positions (Brown-Forsythe test: $F(1) = 1$, $p = 0.3$). Furthermore, we did not find any clear evidence that precipitation or tidal cycle influenced the scattering of the data (Figure S6). We also did not find any relationship between *HI* and estuarine water salinity, pH, dissolved oxygen, temperature, or turbidity (Figure S7).

4.5 Flushing Index

Like *HI*, *FI* was strongly affected by wet/dry seasonality. *FI* was predominantly positive during the wet season (median *FI* = 0.14) and predominantly negative during the dry season (median *FI*= -0.19; Kruskal-Wallis test: H= 29.4, df = 1, p < 0.0001; Figure 7A). The median *FI* was negative for the three marsh positions, with median *FI* values of -0.13, -0.15, and -0.14 for the lower, middle, and upper marsh positions, respectively, and there were no significant differences among the marsh positions (Kruskal-Wallis test: H= 0.007, df = 2, p = 1). Similarly, we did not find significant differences between the 10, 30, and 50 cm depths, with median *FI* values of -0.13, -0.11, and -0.16, respectively (Kruskal-Wallis test: H= 1.02, df = 2, p = 0.6).

The effect of seasonality on *FI* was evident in individual salt marsh positions. In the lower marsh, predominantly negative *FI*s during the dry season (median = -0.20) contrast with positive *FI*s during the wet season (median = 0.11; Kruskal-Wallis test: H= 10.68, df = 1, p = 0.001). However, in the middle marsh, we did not find significant differences between the dry (median *FI* = -0.16) and wet seasons (median *FI* = 0.08; Kruskal-Wallis test: H= 0.27, df = 1, p = 0.6). In the upper marsh, we found significant differences in *FI* between dry (median *FI* = -0.19) and wet periods (median *FI* = 0.19; Kruskal-Wallis test: H= 31.74, df = 1, p < 0.0001).

The wet/dry seasonality effect on *FI* patterns was evident across depth for each individual marsh position (Table 4). In the upper marsh position, wet and dry season *FI*s were significant at all depths (Table 4). In the middle marsh, the effect of seasonality was significant between wet and dry periods for the 10 cm, but not for the 30 or 50 cm depths (Table 4). The lower marsh position had significant differences between wet and dry periods for the 50 cm depth, but not for the 10 or 30 cm depths (Table 4).

Dispersion in *FI* differed significantly between wet and dry periods for the middle (Brown-Forsythe test: F(1) = 29.4, p < 0.001) and upper marsh positions (Brown-Forsythe test: F(1) = 4.5, p < 0.05) with the wet season displaying a larger scattering than the dry season (Figure 7). We did not find significant scattering for the lower marsh (Brown-Forsythe test: F(1) = 0.76, p = 0.4). Moreover, we did not find any clear evidence that precipitation or tidal cycle influenced the scattering of the data (Figure S6). In addition, we did not find any relationship between *FI* and estuarine water salinity, pH, dissolved oxygen, temperature, or turbidity (Figure S8).

Marsh Position	**Depth [cm]**	**median dry season *HI***	**median wet season *HI***	**Kruskal-Wallis**
Lower	10	0.14	-0.03	6.4
Lower	30	0.36	0.16	0.5
Lower	50	0.06	-0.2	4.4
Middle	10	0.16	0.37	3.8
Middle	30	0.06	-0.16	2.7
Middle	50	0.10	0.27	1.4

Upper	10	0.21	-0.28	10.8
Upper	30	0.18	0.01	7.4
Upper	50	0.13	-0.06	4.5
		median dry season *FI*	**median wet season *FI***	**Kruskal-Wallis**
Lower	10	-0.17	0.04	6.4
Lower	30	-0.22	-0.13	0.1
Lower	50	-0.21	0.46	4.9
Middle	10	-0.19	-0.74	6.2
Middle	30	-0.04	0.37	3.3
Middle	50	-0.17	-0.42	0.4
Upper	10	-0.22	-0.26	13.0
Upper	30	-0.19	0.06	9.0
Upper	50	-0.18	0.33	9.3

Table 4. Summary statistics of seasonal effects on hysteresis index (HI) and flushing index (FI) by depth in each marsh position. Significant differences in wet/dry seasons are marked by bolded p-values in the table. All tests in the table have 1 degree of freedom.

5 Discussion

We combined high-frequency NO_3^- concentration and water level time series to calculate NO_3^--subsurface water level hysteresis indices to evaluate the effects of tidal forcings on marsh porewater biogeochemistry over short (diel) timescales, and ultimately understand how precipitation seasonality modulates these short-term relationships. This hysteresis index approach has been widely used in riverine systems (i.e., c-Q plots; (Aguilera & Melack, 2018)), but we adapted it to a coastal setting to provide new insight into how seasonality modulates the role of tidal events in driving porewater NO_3^- dynamics along a salt marsh tidal inundation gradient. We explored how these hydrologic drivers interact to produce seasonal patterns in subsurface chemistry that might influence nutrient export to coastal waters. This analysis can help us understand the potential impacts of climate change, especially the predicted extreme changes in precipitation patterns in the western United States (Swain et al., 2018), that might lead to significant shifts in the porewater NO_3^- concentration dynamics and marsh source/sink status.

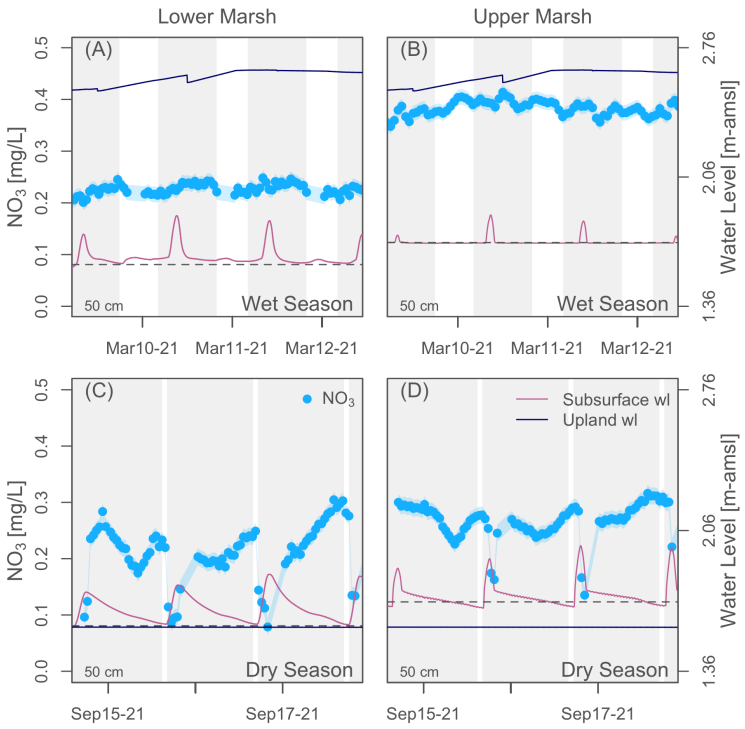

Figure 3. Plot of sub-hourly porewater NO_3^- concentrations from ~4 days during two deployment periods (March 9-12 and September 14-18 2021) from the 50 cm depth at the lower (a and c) and upper (b and d) marsh positions. The shaded regions represent the time intervals that were delineated for individual tidal events. The horizontal dashed lines mark the elevation above mean sea level of the salt marsh platform. The subsurface water level measured in observation wells at each marsh position is shown in pink, and captures the local tidal cycle response. The terrestrial groundwater level measured at an upland position (navy blue line) is shown to highlight the "wetness" of the system as well as the elevation of the terrestrial groundwater with respect to the salt marsh elevation (e.g., high during the wet season and low during the dry season). The light blue envelope on the NO_3^- time series represents the uncertainty of the measurement at 95% confidence level of a linear regression between lab-measurements and the optical probe predictions.

5.1 Seasonal shifts in hysteresis indices

Multi-scale temporal (intra-tidal and seasonal) hydrologic fluxes drive salt marsh porewater NO_3^- dynamics. While diel tidal forcings dominate NO_3^- fluctuations over short periods (Figure 6), the seasonal wet/dry regimes control shifts in the directionality of hysteresis between $NO_3^-$and subsurface water level. Observed *HI* and *FI* values had opposite signs as a function of season (Figure 7). During

the dry season, most tidal events had positive *HI* (clockwise) and negative *FI* (depletion; Figure 7). During the wet season, we observed negative *HI* (counterclockwise) and positive *FI* (production; NO_3^- Figure 7).

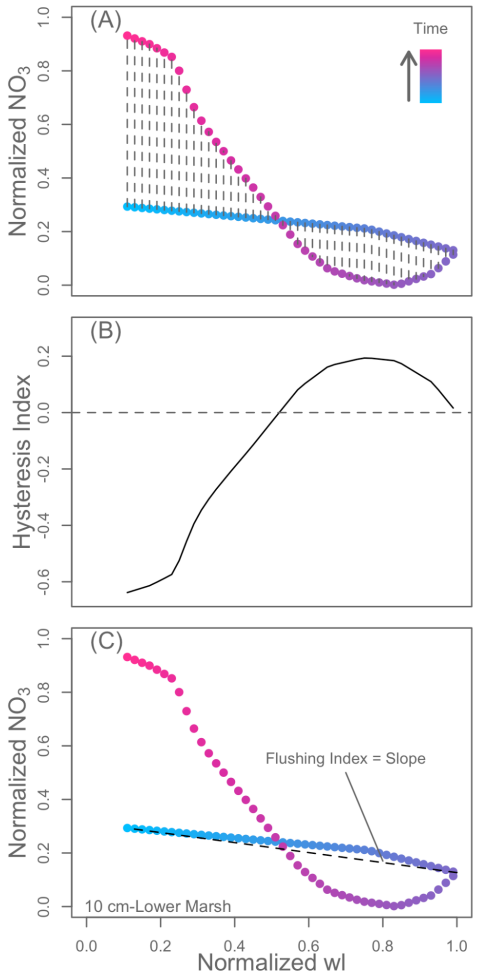

Figure 4. Plots of (a) normalized NO_3^-concentration and normalized water level , (b) hysteresis index (*HI*), and (c) flushing index (FI_i) for a tidal event at the lower marsh position (10 cm depth) on September 19th, 2021. We calculated hysteresis index HI_j (vertical dashed black lines in a) by subtracting the normalized NO_3^- on the falling limb from that of the rising limb for each 1 % of the normalized water level (as illustrated by the dashed lines on A). The event *HI* is the mean HI_j. The *FI* is the slope of the line that intersects the normalized NO_3^- concentration at the beginning and the point of peak water level for each tidal event (c). In this example *HI* = -0.091 and *FI* = -0.19.

For the wet season, the hysteresis results generally imply limited transport of proximal NO_3^- sources early in the tidal event cycle, followed by enrichment from distal and NO_3^--rich sources or in situ production of NO_3^-. Specifically, we observed that the porewater NO_3^- concentration increased after the peak of the tidal event during the wet season. This could result from the oxidation (nitrification) of NH_4^+ stored in the sediment pores, and/or from a rise in the groundwater table (Figure 2), if the groundwater has elevated NO_3^-. In watershed hydrology, where these indices were developed, negative *HI*s and positive *FI*s have been described in golf courses and agricultural areas and were attributed to a rising water table during precipitation events, mobilizing NO_3^- from fertilizer applications stored in upper soil horizons (Aguilera & Melack, 2018; Grande et al., 2019; Oeurng et al., 2010). Our data suggest that similar mechanisms may be mobilizing NO_3^- in coastal wetlands.

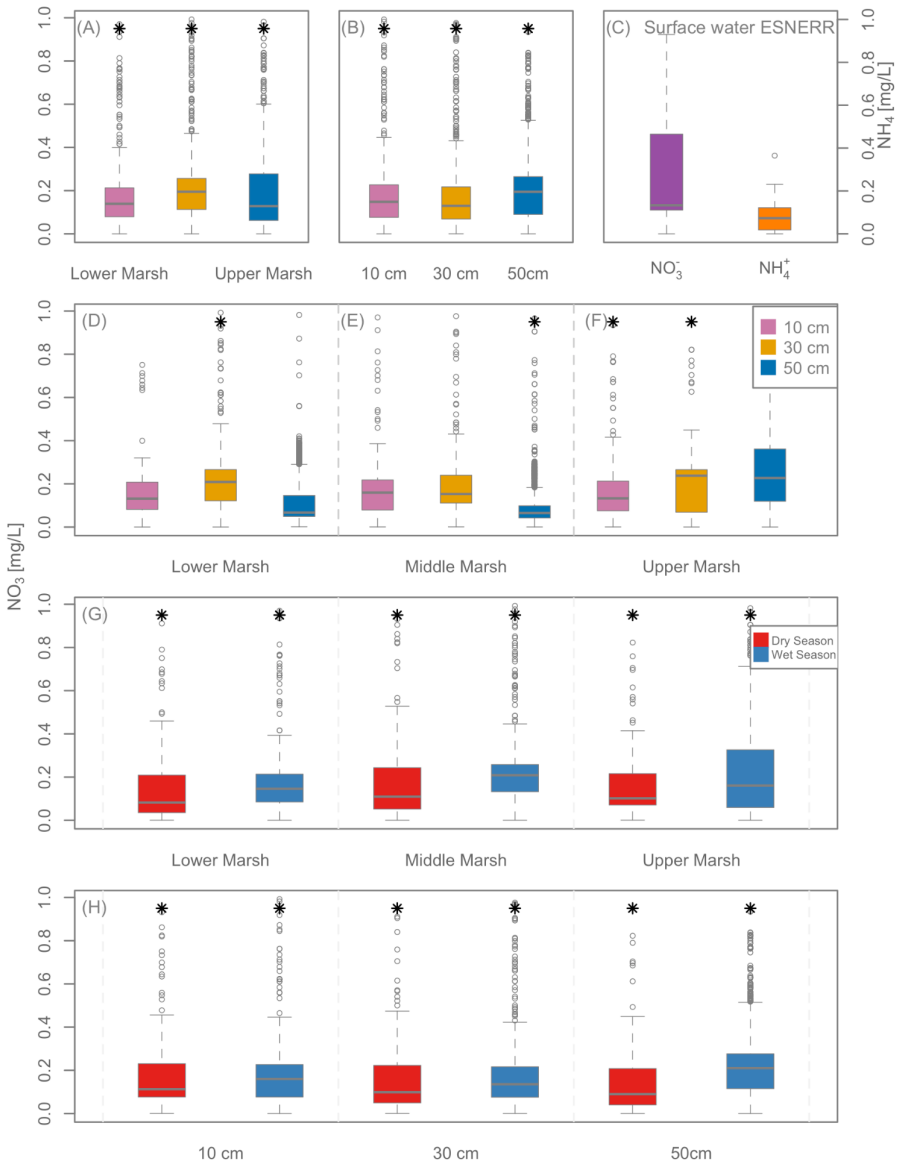

Figure 5. (a) Porewater NO_3^- concentrations across the three marsh positions considering all depths. (b) Marsh porewater NO_3^- concentration at 10, 30, and 50 cm depths for all marsh positions. (c) Plot of NO_3^- and NH_4^+ concentrations from surface water in the ESNERR for the 2021 calendar year. (d), (e), and (f) NO_3^- concentrations across depths for each marsh position. (g) NO_3^- concentration across the three marsh positions separated by dry (red) and wet

seasons (blue). (h) NO_3^- concentration across the three depths separated by dry (red) and wet seasons (blue). One sample in (c) exceeded the 1 mg/L limit of the y axis with a concentration of 2.9 mg/L and was collected in February 2021. Asterisks on top of the plot designate significant differences (p-value $<$ 0.05). All plot ordinates are on the same scale.

The negative hysteresis index values in the wet season suggest that the NO_3^- source, which we hypothesize is dominated by tidally driven estuarine surface water, is progressively removed (i.e., depleted) as it exchanges with the marsh platform (Figure 8). This finding aligns with previous work showing that salt marsh systems can remove NO_3^-, thereby reducing the impacts of excess nutrients on nearshore waters (Bowen et al., 2020; Bulseco et al., 2019; Hamersley & Howes, 2005). Further, previous work in salt marshes has highlighted that NO_3^- is imported from estuarine surface water into marsh porewater during spring and neap tides (Wang et al., 2022).

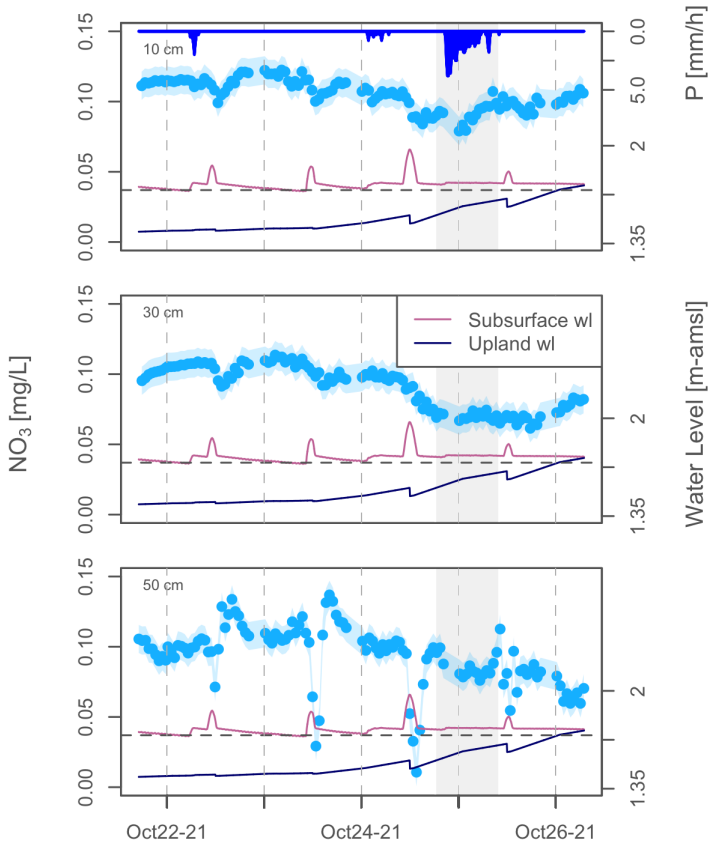

Figure 6. Upper marsh porewater NO_3^- time series during part of the October 2021 deployment for (a) 10 cm, (b) 30 cm, and (c) 50 cm depths. The shaded

region highlights a focal precipitation event observed during this period (notice the inverted hyetograph on top), which disturbed the tidal effect in the NO_3^- time series. The pink line is the subsurface water level, and the dark blue is the terrestrial groundwater level. The figure illustrates how minima in NO_3^- lag the high tides at the 10 cm and 30 cm depths, and a gradual increase in NO_3^- concentration in the low tide. However, we observe a much faster increase in NO_3^- concentration following the high tide at the 50 cm depth. The horizontal dashed line marks the elevation of the salt marsh at this position (1.7 m-amsl).

While different marsh positions experience different inundation extents, the predominant hysteresis index values indicate that all marsh positions share a similar NO_3^--subsurface water level relationship. Overall, tidally driven Elkhorn Slough surface water was the dominant nutrient source to the subsurface (Figure 8). This finding is remarkable, considering that different marsh positions have distinct hydrologic pathways and differing influences of terrestrial groundwater inputs (Robinson et al., 2018). We had previously hypothesized that NO_3^- sources could range from mostly estuarine surface water in the lower marsh to a mix of tidally driven estuarine surface water, terrestrial groundwater, and surface runoff in the upper marsh.

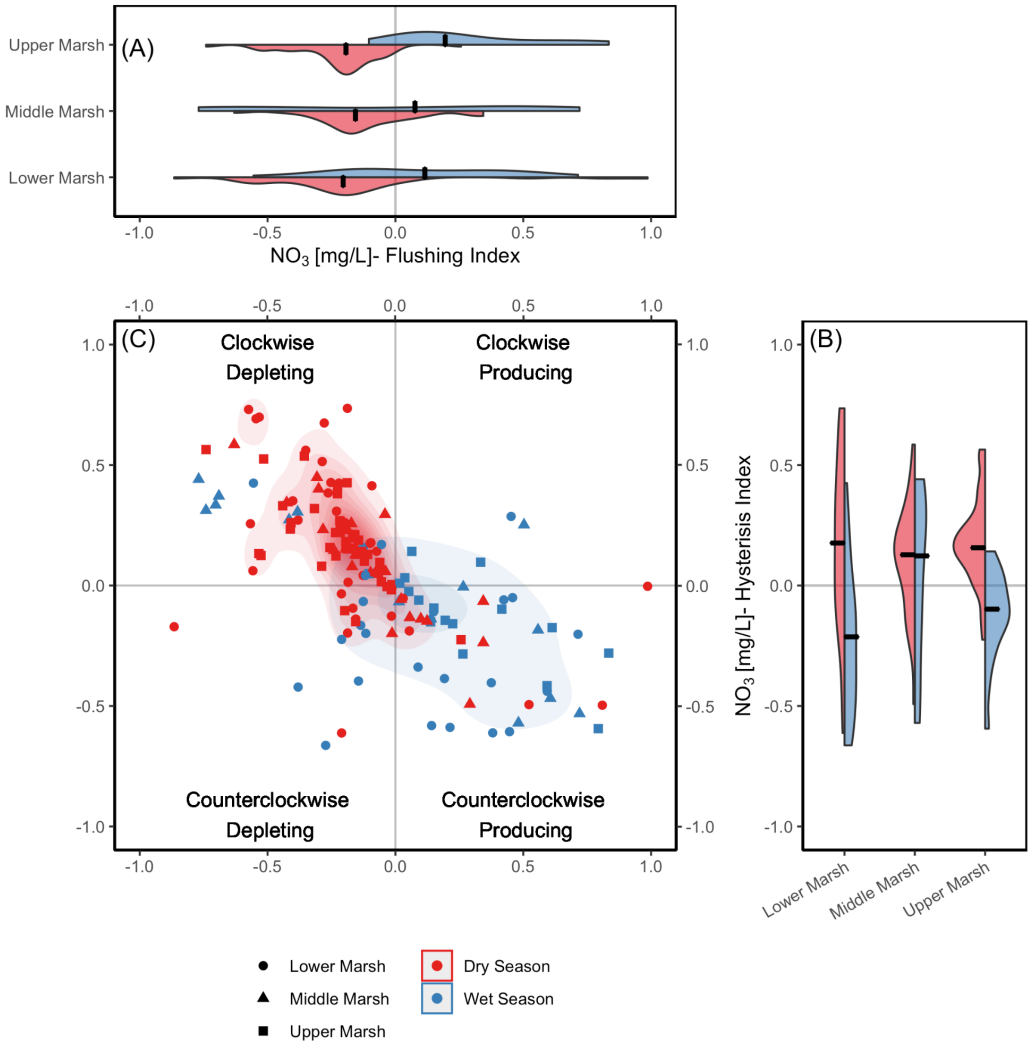

Figure 7. Split violin plots of the (a) tidal event flushing index and (b) hysteresis index for the lower, middle, and upper marsh positions, separated by dry (red) and wet (blue) seasons. The split violin plots show the distribution of hysteresis index values across all tidal events. The black line in each violin plot marks the median of the distribution. (c) The hysteresis index versus flushing index for the 158 tidal events for the lower (circles; 58 events), middle (triangles; 43 events), and upper marsh (squares; 57 events) positions. Separating the hysteresis indices by dry (red) and wet (blue) seasons results in significant differences between these metrics.

Although the hysteresis indices were not significantly different between marsh

positions, we observed differences in the importance of the wet versus dry season in explaining hysteresis indices across different depths. The results for the upper and lower marsh are consistent with the general patterns observed across the salt marsh as a result of seasonality (Figure 7C). In the middle marsh, seasonal patterns did not differ in hysteresis indices among depths. The hysteresis indices in the middle marsh had a large variability across the range of *HI* and *FI* (Figure 7C), with little apparent differences in hysteresis in this marsh position when comparing depths and seasons (Table 4).

Variability in the hysteresis and flushing indices was more pronounced in wet periods than in dry periods (Figure 7). However, we did not find any relationship between *HI* and *FI* and the timing of precipitation events, terrestrial water level elevation, tidal elevation, surface water temperature, surface water pH, surface water salinity, or surface water turbidity (Figures S6, S7, S8). This finding suggests that the variability in *HI* and *FI* during the wet season is likely driven by other processes, such as other NO_3^- delivery mechanisms that our analysis is unable to constrain. Further, these findings could result from a combined effect of these different parameters. Principal component analysis might trase out some overarching influence, but such analysis is beyond the scope of this paper.

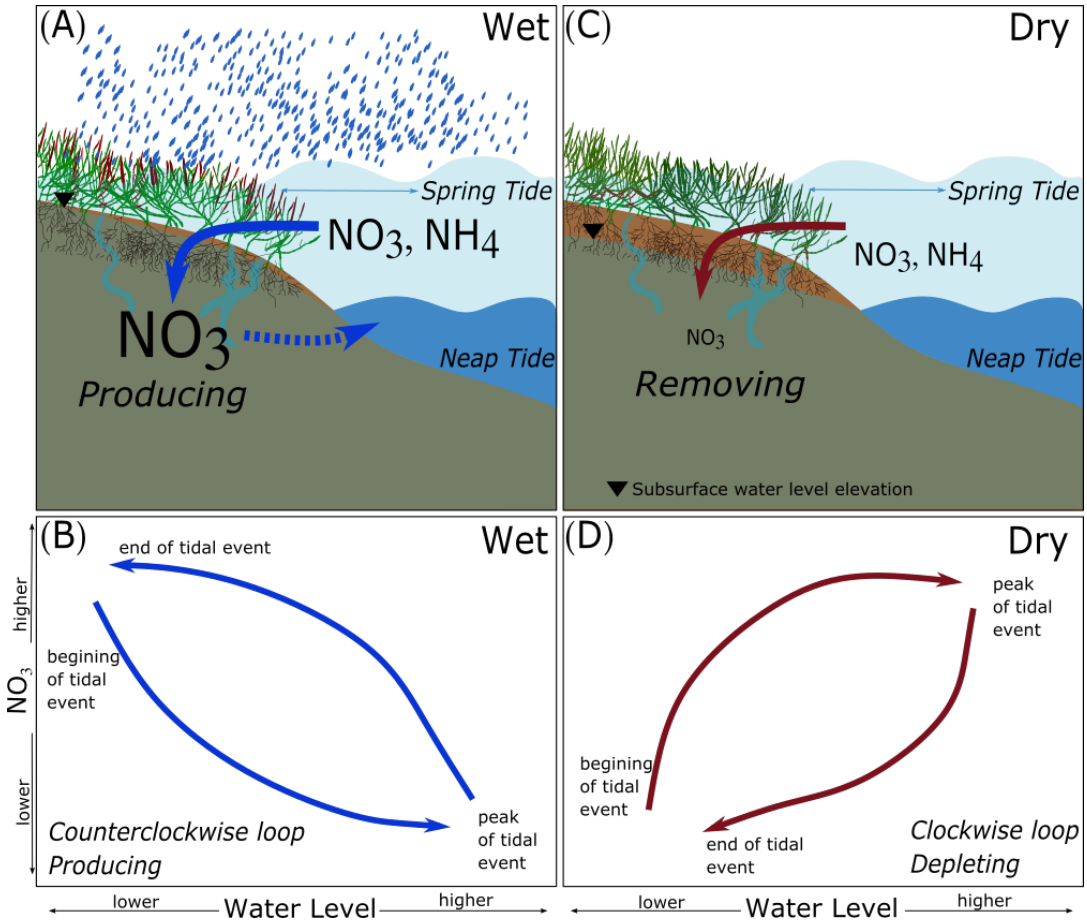

Figure 8. Conceptual model of multi-scale hydrologic drivers (tidal and seasonal) in the salt marsh highlighting the shifts in the biochemical behavior of the salt marsh between wet (a-b) and dry (c-d) seasons. Counterclockwise loops and producing patterns in the wet season indicate that the salt marsh is a NO_3^- source. Clockwise loops and depleting patterns in the dry season show that in this season, the salt marsh is a NO_3^- sink. Notice that surface water nutrient concentrations (NO_3^-, NH_4^+) are higher during the wet season.

5.2 Seasonal effects on porewater nitrate dynamics

Porewater NO_3^- concentrations were predominantly higher during the wet season across depths and marsh positions (Figures 3 and 5D-E). As a result of agricultural runoff into the estuary, significantly higher NO_3^- concentrations are common in surface water during the wet season (Van Dop et al., 2019) and can be an important source of NO_3^- to salt marsh porewater. This contrasts with the dry season, where we observed lower porewater NO_3^- concentrations

for all depths in the lower and middle marsh positions. That said, NO_3^- concentrations were higher during dry periods for the 10 and 30 cm depths in the upper marsh. We suggest that the seasonal wet/dry effect in the upper marsh could result in *in situ* NO_3^- production (nitrification) during dry periods. Considering that the upper marsh is inundated less frequently, and that the dry season occurs in synchrony with the growing season, there is a higher potential for soil aeration that can result in nitrification (Koop-Jakobsen & Giblin, 2010, p.).

The amplitude of NO_3^- fluctuations at intra-tidal scales varied between seasons. During the wet season, the tidal fluctuations of the NO_3^- time series were less evident (i.e., the distinct NO_3^- peaks at tidal frequencies were damped; Figure 3 A-B). When the terrestrial groundwater level was below the marsh surface in the dry season, we observed a stronger tidal signal in the NO_3^- record (Figure 3 C-D). We expected to find the opposite pattern (more significant fluctuations in pore water NO_3^- over wet season tidal cycles) because of higher NO_3^- concentrations in wet season surface water (Van Dop et al., 2019) and because NO_3^- is often limiting in marsh environments (Bledsoe et al., 2020). However, NO_3^- removing patterns in the dry season resulted in a more pronounced intra-tidal variation than the NO_3^--producing behavior in the wet season.

Precipitation events had short-term effects on observed salt marsh porewater NO_3^- concentrations (e.g., Figure 6). For example, in the October deployment, we found that the tidal effect appeared more muted in the NO_3^- time series during precipitation periods across all depths and marsh positions (shaded region in Figure 6), suggesting that precipitation water exchanged with salt marsh porewater, diluting the NO_3^- concentration. This result agrees with previous observations of multilevel decomposition of continuous redox potential measurements across this salt marsh transect during a precipitation event that showed how precipitation water changed redox potential at depth (Grande et al., 2022). These interactions seem to occur at relatively short timescales because we see a relatively instantaneous dilution pattern during the storm event in the NO_3^- time series that recovered quickly.

5.3 Intra-tidal and spatial effects on marsh porewater nitrate concentration

While seasonality was the key driver of porewater NO_3^- concentrations across the marsh, we observed within-marsh variation across tidal events, positions, and depths (Figures 3 and 5).Tidal events influenced porewater NO_3^- concentrations on hourly timescales across the study period, with distinct NO_3^- spikes (both positive and negative) at tidal frequencies across depths and marsh positions (e.g., Figures 3 and 6). These findings are consistent with previous measurements of high-frequency (1-minute resolution) redox potential and subsurface water level that suggested a relatively fast exchange of tidal water with porewater that influenced biogeochemical processes at intra-tidal timescales (Grande et al., 2022). We observed a tidal "signature" consisting of a characteristic in-

crease and subsequent decrease in porewater NO_3^- during inundation (Figure 6). One possibility is NO_3^- in tidal surface water infiltrates into the marsh subsurface and is subsequently consumed by dissimilatory nitrate reduction processes such as denitrification or DNRA (Devol, 2015; Giblin et al., 2013). Alternatively, Elkhorn Slough surface water has relatively elevated NH_4^+ concentration (Hicks et al., 2019), which in combination with dissolved oxygen in tidal waters, can lead to nitrification in the marsh subsurface (i.e., the salt marsh can be a source of NO_3^-). Similarly, we observed small-scale within-marsh variation across positions and depths. Microbial processes such as dissimilatory nitrate reduction or nitrification are tightly coupled to plant activity, oxygen concentrations, and substrate availability (Koop-Jakobsen & Wenzhöfer, 2015). Although our study does not address the direct mechanisms causing variation in NO_3^- concentrations, our in situ high-frequency sensor measurements indicate that within-marsh processing exerts influence on net marsh NO_3^- export within the broader context of seasonal hydrologic drivers. Further, our findings highlight the importance of short-term and small-scale drivers of NO_3^- dynamics that might not be captured with point or synoptic measurements.

5.4 Implications for salt marsh biogeochemistry

The analysis presented here illustrates the potential benefit of continuous high-spatiotemporal resolution water quality data in combination with methods to quantify tidal event hysteresis in salt marsh environments. Salt marshes are under pressure from chronic sea level rise and increasing human activity around coastal environments (Krause et al., 2020). Although biogeochemical cycling of NO_3^- and other nitrogen species on coastal wetlands have been studied extensively (Bowen et al., 2020), NO_3^- processing at intra-tidal time scales across different depths is not often considered.

The hysteresis indices used in this study indicate that the salt marsh has different dominant transport and biogeochemical processing behavior in wet and dry seasonal periods (Figure 7). Overall, the salt marsh is most retentive during the dry season, and depletion and consumption patterns dominate during these periods, whereas the salt marsh is least retentive during the wet season when NO_3^- production dominates. This is particularly evident in the lower and upper marsh positions, where the salt marsh shifts between predominantly removing NO_3^- in dry periods and producing NO_3^- in wet periods.

These marked differences in the overall NO_3^- processing in the salt marsh as a function of seasonality may become more evident with changing patterns in precipitation (Donat et al., 2016). Climate change in California is projected to cause less frequent, but more intense precipitation events (Swain et al., 2018), which is observed to already be affecting salt marsh functionality (Russo et al., 2013). Fewer, but more extreme precipitation events will likely result in relatively higher pulses of NO_3^- into the estuary during runoff events because NO_3^- will probably accumulate in the soil during extended rainless periods and get flushed during higher intensity storm events. Predicted higher NO_3^- loads

to Elkhorn Slough will test the potential of the salt marsh to remove pollutants and improve water quality in coastal systems.

6 Conclusions

This study identified the role of multi-scale (intra-tidal and seasonal) hydrologic drivers on controlling porewater NO_3^- concentrations in a Mediterranean-climate salt marsh system, where water quality is a concern. Overall, the knowledge obtained from this analysis of NO_3^- hysteretic responses to tidal events is valuable in providing insight into solute-subsurface water level patterns that occur at different depths and marsh positions/elevations. The seasonal differences in NO_3^- dynamics over sub-hourly timescales highlight the significance of both long-term and high frequency continuous monitoring.

As global climate shifts, factors including sea-level rise will induce changes in marsh position functioning and ecological services. We used a relatively simple and robust methodology for evaluating key marsh biogeochemical processes. The methods presented here can assist in interpreting coastal hydro-biochemical processes, which can help with the urgency to predict future scenarios under sea-level rise conditions. Further, applying these techniques has potential transformative influence on our knowledge of coupled hydrological and biogeochemical processes in marsh ecosystems.

Future work should consider longer instrument deployment and monitoring periods, particularly during the wet season, because the majority of the tidal events captured by this study corresponded to dry periods, and ideally across a range of wet, normal, and dry climate periods. More extended studies will help to resolve the role of varied hydrologic inputs, including runoff from agricultural activities and storm events. Further, similar studies in other coastal systems, including other salt marshes in different climatic regions, are needed to put these findings into a comprehensive context. By integrating sites with varying degrees of tidal inundation and tidal patterns (e.g., diurnal and semidiurnal), we could better isolate tidal inundation from other salt marsh biochemical processes.

Our future work will incorporate these high spatiotemporal field measurements of NO_3^- concentrations with additional monitoring data of salinity and isotopic fingerprints to understand mixing between terrestrial groundwater and inundation. An essential remaining step in the field is to implement these hydro-biogeochemical processes into reactive transport modeling to develop practical mechanistic understanding, including explaining the interactions between flow paths, residence times, and solute kinetics in coastal systems. We think that an integrative understanding of physical and biogeochemical processes will be crucial for managing salt marshes as NO_3^- enrichment and sea-level rise continue to threaten our coasts.

Acknowledgments

The authors sincerely thank Dan Sampson from the University of California Santa Cruz (UCSC) for his valuable help programming and installing the elec-

tronic devices used in this study. We also thank Dr. Brian Dreyer, director of the Marine Analytical Lab at UCSC for help with sample analysis. We thank Maya Montalvo, Loren Tolley-Man, Michael Wilshire, and Andria Greene for field assistance. EG was partially funded by a Cota-Robles Fellowship through the University of California Santa Cruz and by a NOAA Margaret A. Davidson fellowship (NA20NOS4200122). We acknowledge support from the NITRATES Project, funded by the U.S. Department of Energy, Office of Science, Office of Biological and Environmental Research, Award Number DE-SC0021044. We acknowledge support from a California SeaGrant under California Natural Resources Agency Award Number C0303100.

Open Research

The nitrate and water level time series data used in the manuscript will be uploaded to the ESS-DIVE DOE repository on acceptance.

References

Addy, K., Gold, A., Nowicki, B., McKenna, J., Stolt, M., & Groffman, P. (2005). Denitrification capacity in a subterranean estuary below a Rhode Island fringing salt marsh. *Estuaries*, *28*(6), 896–908. https://doi.org/10.1007/BF02696018Aguilera, R., & Melack, J. M. (2018). Concentration-Discharge Responses to Storm Events in Coastal California Watersheds: C-Q STORM RESPONSES COASTAL CALIFORNIA. *Water Resources Research*, *54*(1), 407–424. https://doi.org/10.1002/2017WR021578Almaraz, M., Wong, M. Y., & Yang, W. H. (2020). Looking back to look ahead: a vision for soil denitrification research. *Ecology*, *101*(1), e02917. https://doi.org/10.1002/ecy.2917Andrea, B., Francesc, G., Jérôme, L., Eusebi, V., & Francesc, S. (2006). Cross-site Comparison of Variability of DOC and Nitrate c–q Hysteresis during the Autumn–winter Period in Three Mediterranean Headwater Streams: A Synthetic Approach. *Biogeochemistry*, *77*(3), 327–349. https://doi.org/10.1007/s10533-005-0711-7Arora, B., Burrus, M., Newcomer, M., Steefel, C. I., Carroll, R. W. H., Dwivedi, D., et al. (2020). Differential C-Q Analysis: A New Approach to Inferring Lateral Transport and Hydrologic Transients Within Multiple Reaches of a Mountainous Headwater Catchment. *Frontiers in Water*, *2*. Retrieved from https://www.frontiersin.org/article/10.3389/frwa.2020.00024Beheshti, K., Endris, C., Goodwin, P., Pavlak, A., & Wasson, K. (2022). Burrowing crabs and physical factors hasten marsh recovery at panne edges. *PLOS ONE*, *17*(1), e0249330. https://doi.org/10.1371/journal.pone.0249330Bieroza, M. Z., & Heathwaite, A. L. (2015). Seasonal variation in phosphorus concentration–discharge hysteresis inferred from high-frequency in situ monitoring. *Journal of Hydrology*, *524*, 333–347. https://doi.org/10.1016/j.jhydrol.2015.02.036Birgand, F., Aveni-Deforge, K., Smith, B., Maxwell, B., Horstman, M., Gerling, A. B., & Carey, C. C. (2016). First report of a novel multiplexer pumping system coupled to a water quality probe to collect high temporal frequency in situ water chemistry measurements at multiple sites: High-Resolution Water Chemistry in Time and Space. *Limnology and Oceanography: Methods*, *14*(12), 767–783.

https://doi.org/10.1002/lom3.10122Bledsoe, R. B., Bean, E. Z., Austin, S. S., & Peralta, A. L. (2020). A microbial perspective on balancing trade-offs in ecosystem functions in a constructed stormwater wetland. *Ecological Engineering*, *158*, 106000. https://doi.org/10.1016/j.ecoleng.2020.106000Bowen, J. L., Giblin, A. E., Murphy, A. E., Bulseco, A. N., Deegan, L. A., Johnson, D. S., et al. (2020). Not All Nitrogen Is Created Equal: Differential Effects of Nitrate and Ammonium Enrichment in Coastal Wetlands. *BioScience*, *70*(12), 1108–1119. https://doi.org/10.1093/biosci/biaa140Bulseco, A. N., Giblin, A. E., Tucker, J., Murphy, A. E., Sanderman, J., Hiller-Bittrolff, K., & Bowen, J. L. (2019). Nitrate addition stimulates microbial decomposition of organic matter in salt marsh sediments. *Global Change Biology*, gcb.14726. https://doi.org/10.1111/gcb.14726Caetano, M., Bernárdez, P., Santos-Echeandia, J., Prego, R., & Vale, C. (2012). Tidally driven N, P, Fe and Mn exchanges in salt marsh sediments of Tagus estuary (SW Europe). *Environmental Monitoring and Assessment*, *184*(11), 6541–6552. https://doi.org/10.1007/s10661-011-2439-2Caffrey, J. M. (2002). Chapter 3: Climate. In J. M. Caffrey, M. Brown, B. Tyler, & M. Silberstain (Eds.), *Changes in a California estuary: An ecosystem profile of Elkhorn Slough* (pp. 25–28). Moss Landing, California: Elkhorn Slough Fundation. Retrieved from http://library.elkhornslough.org/attachments/Caffrey_2002_Changes_In_A_California.pdfCaffrey, J. M., & Broenkow, W. (2002). Chapter 4: Hydrography. In J. M. Caffrey, M. Brown, B. Tyler, & M. Silberstain (Eds.), *Changes in a California estuary: An ecosystem profile of Elkhorn Slough* (pp. 29–42). Moss Landing, California: Elkhorn Slough Fundation. Retrieved from http://library.elkhornslough.org/attachments/Caffrey_2002_Changes_In_A_California.pdfCaffrey, Jane M., Harrington, N., & Ward, B. (2002). Biogeochemical processes in a small California estuary. 1. Benthic fluxes and pore water constituents reflect high nutrient freshwater inputs. *Marine Ecology Progress Series*, *233*, 39–53. https://doi.org/10.3354/meps233039Chanat, J. G., Rice, K. C., & Hornberger, G. M. (2002). Consistency of patterns in concentration-discharge plots: PATTERNS IN CONCENTRATION-DISCHARGE PLOTS. *Water Resources Research*, *38*(8), 22-1-22–10. https://doi.org/10.1029/2001WR000971Chapin, T. P., Caffrey, J. M., Jannasch, H. W., Coletti, L. J., Haskins, J. C., & Johnson, K. S. (2004). Nitrate sources and sinks in Elkhorn Slough, California: Results from long-term continuous in situ nitrate analyzers. *Estuaries*, *27*(5), 882–894. https://doi.org/10.1007/BF02912049Devol, A. H. (2015). Denitrification, Anammox, and N2 Production in Marine Sediments. *Annual Review of Marine Science*, *7*(1), 403–423. https://doi.org/10.1146/annurev-marine-010213-135040Donat, M. G., Lowry, A. L., Alexander, L. V., O'Gorman, P. A., & Maher, N. (2016). More extreme precipitation in the world's dry and wet regions. *Nature Climate Change*, *6*(5), 508–513. https://doi.org/10.1038/nclimate2941Etheridge, J. R., Birgand, F., Osborne, J. A., Osburn, C. L., Burchell, M. R., & Irving, J. (2014). Using in situ ultraviolet-visual spectroscopy to measure nitrogen, carbon, phosphorus, and suspended solids concentrations at a high frequency in a brackish tidal marsh: In situ spectroscopy to monitor N, C, P, TSS. *Limnology and Oceanogra-*

phy: Methods, *12*(1), 10–22. https://doi.org/10.4319/lom.2014.12.10Giblin, A., Tobias, C., Song, B., Weston, N., Banta, G., & Rivera-Monroy, V. (2013). The Importance of Dissimilatory Nitrate Reduction to Ammonium (DNRA) in the Nitrogen Cycle of Coastal Ecosystems. *Oceanography*, *26*(3), 124–131. https://doi.org/10.5670/oceanog.2013.54Grande, E., Visser, A., Beitz, P., & Moran, J. (2019). Examination of Nutrient Sources and Transport in a Catchment with an Audubon Certified Golf Course. *Water*, *11*(9), 1923. https://doi.org/10.3390/w11091923Grande, E., Arora, B., Visser, A., Montalvo, M., Braswell, A., Seybold, E., et al. (2022). Tidal frequencies and quasiperiodic subsurface water level variations dominate redox dynamics in a salt marsh system. *Hydrological Processes*, *36*(5), 1–16. https://doi.org/10.1002/hyp.14587Hamersley, M. R., & Howes, B. L. (2005). Coupled nitrification–denitrification measured in situ in a Spartina alterniflora marsh with a 15NH4+ tracer. *Marine Ecology Progress Series*, *299*, 123–135. https://doi.org/10.3354/meps299123Hicks, K., Jeppesen, R., Haskins, J., & Wasson, K. (2019). *Long-term trends and spatial patterns of water quality in estuarine wetlands of central California. Elkhorn Slough Technical Report Series* (Scientific Report No. 2019:1). Moss Landing, California: Elkohrn Slough NERR. Retrieved from http://library.elkhornslough.org/research/bibliography/Hicks_2019_Long-term_trends_and_spatial.pdfHughes, B. B., Haskins, J. C., Wasson, K., & Watson, E. (2011). Identifying factors that influence expression of eutrophication in a central California estuary. *Marine Ecology Progress Series*, *439*, 31–43. https://doi.org/10.3354/meps09295Jeppesen, R., Rodriguez, M., Rinde, J., Haskins, J., Hughes, B., Mehner, L., & Wasson, K. (2018). Effects of Hypoxia on Fish Survival and Oyster Growth in a Highly Eutrophic Estuary. *Estuaries and Coasts*, *41*(1), 89–98. https://doi.org/10.1007/s12237-016-0169-yKincaid, D. W., Seybold, E. C., Adair, E. C., Bowden, W. B., Perdrial, J. N., Vaughan, M. C. H., & Schroth, A. W. (2020). Land Use and Season Influence Event-Scale Nitrate and Soluble Reactive Phosphorus Exports and Export Stoichiometry from Headwater Catchments. *Water Resources Research*, *56*(10), e2020WR027361. https://doi.org/10.1029/2020WR027361Koop-Jakobsen, K., & Giblin, A. E. (2010). The effect of increased nitrate loading on nitrate reduction via denitrification and DNRA in salt marsh sediments. *Limnology and Oceanography*, *55*(2), 789–802. https://doi.org/10.4319/lo.2010.55.2.0789Koop-Jakobsen, K., & Wenzhöfer, F. (2015). The Dynamics of Plant-Mediated Sediment Oxygenation in Spartina anglica Rhizospheres—a Planar Optode Study. *Estuaries and Coasts*, *38*(3), 951–963. https://doi.org/10.1007/s12237-014-9861-yKrause, J. R., Watson, E. B., Wigand, C., & Maher, N. (2020). Are Tidal Salt Marshes Exposed to Nutrient Pollution more Vulnerable to Sea Level Rise? *Wetlands*, *40*(5), 1539–1548. https://doi.org/10.1007/s13157-019-01254-8Kumar, P., Dasgupta, R., Johnson, B. A., Saraswat, C., Basu, M., Kefi, M., & Mishra, B. K. (2019). Effect of Land Use Changes on Water Quality in an Ephemeral Coastal Plain: Khambhat City, Gujarat, India. *Water*, *11*(4), 724. https://doi.org/10.3390/w11040724Liland, K. H., Mevik, B., Wehrens, R., & Hiemstra, P. (2021). pls: Partial Least

Squares and Principal Component Regression (Version 2.8). Retrieved from https://github.com/khliland/plsLiu, W., Youssef, M. A., Birgand, F. P., Chescheir, G. M., Tian, S., & Maxwell, B. M. (2020). Processes and mechanisms controlling nitrate dynamics in an artificially drained field: Insights from high-frequency water quality measurements. *Agricultural Water Management*, *232*, 106032. https://doi.org/10.1016/j.agwat.2020.106032Liu, W., Birgand, F., Tian, S., & Chen, C. (2021). Event-scale hysteresis metrics to reveal processes and mechanisms controlling constituent export from watersheds: A review . *Water Research*, *200*, 117254. https://doi.org/10.1016/j.watres.2021.117254Lloyd, C. E. M., Freer, J. E., Johnes, P. J., & Collins, A. L. (2016). Using hysteresis analysis of high-resolution water quality monitoring data, including uncertainty, to infer controls on nutrient and sediment transfer in catchments. *Science of The Total Environment*, *543*, 388–404. https://doi.org/10.1016/j.scitotenv.2015.11.028Malzone, C. M. (1999). *Tidal scour and its relation to erosion and sediment transport in Elkhorn Slough* (Master Thesis). San Jose State University, San Jose, California, United States.O'Dell, J. W. (1996). DETERMINATION OF NITRATE-NITRITE NITROGEN BY AUTOMATED COLORIMETRY. In *Methods for the Determination of Metals in Environmental Samples* (pp. 464–478). Elsevier. https://doi.org/10.1016/B978-0-8155-1398-8.50026-4Oeurng, C., Sauvage, S., & Sánchez-Pérez, J.-M. (2010). Temporal variability of nitrate transport through hydrological response during flood events within a large agricultural catchment in south-west France. *Science of The Total Environment*, *409*(1), 140–149. https://doi.org/10.1016/j.scitotenv.2010.09.006Peterson, R. N., Moore, W. S., Chappel, S. L., Viso, R. F., Libes, S. M., & Peterson, L. E. (2016). A new perspective on coastal hypoxia: The role of saline groundwater. *Marine Chemistry*, *179*, 1–11. https://doi.org/10.1016/j.marchem.2015.12.005Reading, M. J., Santos, I. R., Maher, D. T., Jeffrey, L. C., & Tait, D. R. (2017). Shifting nitrous oxide source/sink behaviour in a subtropical estuary revealed by automated time series observations. *Estuarine, Coastal and Shelf Science*, *194*, 66–76. https://doi.org/10.1016/j.ecss.2017.05.017Robinson, C. E., Xin, P., Santos, I. R., Charette, M. A., Li, L., & Barry, D. A. (2018). Groundwater dynamics in subterranean estuaries of coastal unconfined aquifers: Controls on submarine groundwater discharge and chemical inputs to the ocean. *Advances in Water Resources*, *115*, 315–331. https://doi.org/10.1016/j.advwatres.2017.10.041Russo, T. A., Fisher, A. T., & Winslow, D. M. (2013). Regional and local increases in storm intensity in the San Francisco Bay Area, USA, between 1890 and 2010: STORM INTENSITY IN THE SFBA. *Journal of Geophysical Research: Atmospheres*, *118*(8), 3392–3401. https://doi.org/10.1002/jgrd.50225Santos, I. R., Eyre, B. D., & Huettel, M. (2012). The driving forces of porewater and groundwater flow in permeable coastal sediments: A review. *Estuarine, Coastal and Shelf Science*, *98*, 1–15. https://doi.org/10.1016/j.ecss.2011.10.024Sinha, E., Michalak, A. M., & Balaji, V. (2017). Eutrophication will increase during the 21st century as a result of precipitation changes. *Science*, *357*(6349), 405–408. https://doi.org/10.1126/science.aan2409Swain, D. L., Langenbrunner, B., Neelin, J. D., & Hall, A. (2018). Increasing precipitation volatility

in twenty-first-century California. *Nature Climate Change*, *8*(5), 427–433. https://doi.org/10.1038/s41558-018-0140-yVan Dop, M., Hall, A., Calhoun, K., & Kislik, C. (2019). *Linking land cover and water quality in Elkhorn Slough. Elkhorn Slough Technical Report Series*. Elkhorn Slough, CA. Retrieved from http://library.elkhornslough.org/attachments/VanDop_2019_Linking_Land_Cover_And.pdfVan Dyke, E., & Wasson, K. (2005). Historical ecology of a central California estuary: 150 years of habitat change. *Estuaries*, *28*(2), 173–189. https://doi.org/10.1007/BF02732853Vaughan, M. C. H., Bowden, W. B., Shanley, J. B., Vermilyea, A., Sleeper, R., Gold, A. J., et al. (2017). High-frequency dissolved organic carbon and nitrate measurements reveal differences in storm hysteresis and loading in relation to land cover and seasonality. *Water Resources Research*, *53*(7), 5345–5363. https://doi.org/10.1002/2017WR020491Wang, F., Xiao, K., Santos, I. R., Lu, Z., Tamborski, J., Wang, Y., et al. (2022). Porewater exchange drives nutrient cycling and export in a mangrove-salt marsh ecotone. *Journal of Hydrology*, *606*, 127401. https://doi.org/10.1016/j.jhydrol.2021.127401Woolfolk, A., & Labadie, Q. (2012). *The significance of pickleweed-dominated tidal salt marsh in Elkhorn Slough, California: A literature review* (Technical Report Series). Elkhorn Slough.Zuecco, G., Penna, D., Borga, M., & van Meerveld, H. J. (2016). A versatile index to characterize hysteresis between hydrological variables at the runoff event timescale: A Hysteresis Index for Variables at the Runoff Event Timescale. *Hydrological Processes*, *30*(9), 1449–1466. https://doi.org/10.1002/hyp.10681